

PCCP

Accepted Manuscript



This is an *Accepted Manuscript*, which has been through the Royal Society of Chemistry peer review process and has been accepted for publication.

Accepted Manuscripts are published online shortly after acceptance, before technical editing, formatting and proof reading. Using this free service, authors can make their results available to the community, in citable form, before we publish the edited article. We will replace this *Accepted Manuscript* with the edited and formatted *Advance Article* as soon as it is available.

You can find more information about *Accepted Manuscripts* in the [Information for Authors](#).

Please note that technical editing may introduce minor changes to the text and/or graphics, which may alter content. The journal's standard [Terms & Conditions](#) and the [Ethical guidelines](#) still apply. In no event shall the Royal Society of Chemistry be held responsible for any errors or omissions in this *Accepted Manuscript* or any consequences arising from the use of any information it contains.

Cite this: DOI: 10.1039/c0xx00000x

www.rsc.org/pccp

PAPER

Reversible addition of the OH radical to p-cymene in the gas phase: multiple adduct formation. Part 2

Paulo Alarcón^a, Birger Bohn^b, Cornelius Zetzsch^{*ac}, Marie-Thérèse Rayez^{*d}, Jean-Claude Rayez^{*d}

Received (in XXX, XXX) Xth XXXXXXXXX 20XX, Accepted Xth XXXXXXXXX 20XX

DOI: 10.1039/b000000x

A flash photolysis – resonance fluorescence (FP-RF) system was used to study the p-cymene (PC) + OH reaction at temperatures between 299 and 349 K in helium. Triexponential functions were fitted to groups of observed OH decay curves according to a model considering a reversible addition to form two adducts as thermolabile reservoirs of OH. Compared to Part 1 of this paper, consideration of a second adduct strongly improved the fits to our measurements, and the rate constants for the major pathways were optimized between 299 and 349 K. The Arrhenius expression for the rate constant of the sum of OH addition and H-atom abstraction pathways was found to be $k_{OH} = 1.9 \times 10^{-12} \exp [(610 \pm 210) \text{ K}/T] \text{ cm}^3 \text{ s}^{-1}$. Rate constants of unimolecular decomposition reactions of the adducts were similar to other aromatic compounds with the following Arrhenius expressions: $1 \times 10^{12} \exp [(-7600 \pm 800) \text{ K}/T] \text{ s}^{-1}$ for adduct 1 and $4 \times 10^{11} \exp [(-8000 \pm 300) \text{ K}/T] \text{ s}^{-1}$ for adduct 2. Adduct yields increased and decreased with temperature for adduct 1 and 2, respectively, but were similar (~ 0.4) around room temperature. Equilibrium constants yielded values for reaction enthalpies and entropies of adduct formations. While for one adduct reasonable agreement was obtained with theoretical predictions, there were significant deviations for the other adduct. This indicates the presence of more than two adduct isomers that were not accounted for in the reaction model. Quantum chemical calculations (DFT M06-2X/6-31G(d,p)) and RRKM kinetics were performed with the aim of clarifying the mechanism of the OH addition to PC. These calculations show that formation of adducts with OH in ortho positions to the isopropyl and methyl substituents is predominant (55% and 24%) to those with OH in ipso positions (21% and 3%). A large fraction ($>90\%$) of the ipso- C_3H_7 adduct is predicted to react by dealkylation forming p-cresol (in the absence of oxygen) and isopropyl radicals. These theoretical results agree well with the interpretation of the experimental results showing that the two ortho adducts (which appeared as OH reservoirs in the experiment) have been observed.

1. Introduction

Non methane volatile organic compounds (NMVOCs) are emitted into the atmosphere by anthropogenic and biogenic sources. It has been estimated that globally biogenic emissions significantly exceed anthropogenic emissions.^{1, 2} NMVOCs play a major role in the photochemical formation of ozone and secondary organic aerosols, and both processes are initiated by OH radicals, NO_3 radicals and O_3 oxidation.^{3, 4}

^a Atmospheric Chemistry Research Laboratory, University of Bayreuth, 95448, Germany.

^b Institut für Energie- und Klimaforschung IEK-8: Troposphäre,

Forschungszentrum Jülich, 52425 Jülich, Germany.

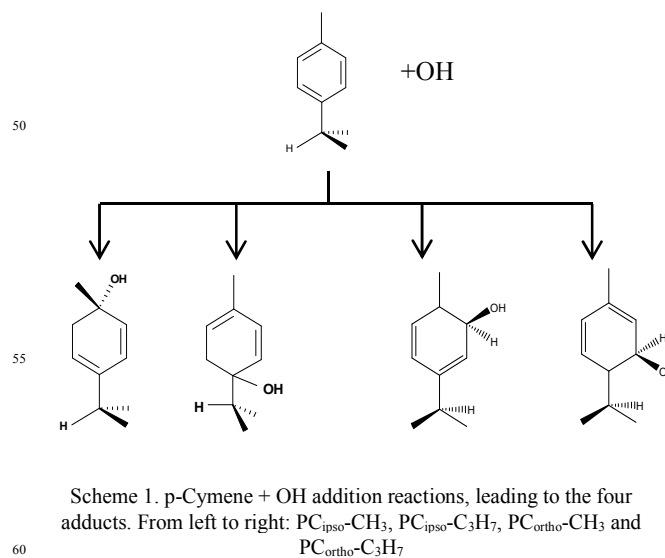
^c Fraunhofer Institute for Toxicology and Experimental Medicine, 30625 Hannover, Germany.

E-mail: cornelius.zetzsch@uni-bayreuth.de

^d Université de Bordeaux, Institut des Sciences Moléculaires, ISM UMR

5255, 33405 Talence, France.

E-mail : mt.rayez@ism.u-bordeaux1.fr and jc.rayez@ism.u-bordeaux1.fr



Cite this: DOI: 10.1039/c0xx00000x

www.rsc.org/pccp

PAPER

The biogenic aromatic compound p-cymene (1-methyl-4-isopropylbenzene or 4-isopropyltoluene) has four distinguishable positions where the OH radicals may add to the aromatic ring, as illustrated in scheme 1: two equivalent ones ortho to the isopropyl group ($\text{PC}_{\text{ortho}}\text{-C}_3\text{H}_7$), two equivalent ones ortho to the methyl group ($\text{PC}_{\text{ortho}}\text{-CH}_3$), and two non-equivalent ipso positions at the site of the methyl and the isopropyl group ($\text{PC}_{\text{ipso}}\text{-CH}_3$ and $\text{PC}_{\text{ipso}}\text{-C}_3\text{H}_7$). Addition to an already occupied position (ipso-addition) is in general considered to be less important, but triexponential decays of OH have been observed by VUV flash photolysis/resonance fluorescence (FP-RF) in the presence of 1,3,5-trimethylbenzene, indicating that two different thermolabile adducts can regenerate OH.⁵ The observation of hexamethyl-2,4-cyclohexadienone by GC-MS as the only product from the reaction of OH with hexamethylbenzene in the presence of NO_2 implies that an addition of OH is a major first step of this reaction.⁶ Biexponential FP-RF-decays of OH in the presence of hexamethylbenzene as a prototype molecule, where ipso positions alone are available for addition, demonstrated a reversible reaction,⁷ and the molecular ion of the adduct has been observed by single-photon VUV photoionization as an intermediate in a flow reactor very recently.⁸ Ipso-type adducts may react by dealkylation and corresponding products from the reaction of toluene, o-, m-, and p-xylene with OH radicals have been observed by chemical ionization mass spectrometry in a flowtube study (5.4% phenol from toluene and similar yields of the cresols expected from dealkylation of the xylenes).⁹ However, these results are not in agreement with an earlier smog chamber result of a phenol yield $< 0.1\%$ from OH + toluene¹⁰ and are not confirmed in a more recent smog chamber study with GC-FID analysis¹¹ that stated an upper limit of $< 1\%$ formation of each cresol from OH + m-xylene and $< 2\%$ for each cresol isomer from OH + p-cymene.

A total OH rate constant of $(15.1 \pm 4.1) \times 10^{-12} \text{ cm}^3 \text{ s}^{-1}$ was derived in a previous study on p-cymene¹² in a smog chamber at room temperature and 1 atm pressure of air. In another work,¹¹ the rate constant of H-atom abstraction was determined measuring the 4-methylacetophenone yield (the major product formed subsequent to the H-atom abstraction from the isopropyl substituent) and assuming a H-atom abstraction rate constant from the methyl substituent similar to the one determined for toluene. This led to an estimated $20 \pm 4\%$ contribution of abstraction to the overall OH rate constant. In our previous work,¹³ the p-cymene + OH reaction was studied over a wide temperature range assuming a single adduct formation (biexponential model). This simplification was found to be satisfactory for temperatures below 320 K and higher than about 350 K, but between these temperatures our applied model could not describe the data. A preliminary study of the OH decay curves in the intermediate temperature range revealed that triexponential functions led to better fits to groups of observed curves than biexponential ones, indicating that more than one adduct was being formed. A similar behaviour has been observed

for 1,3,5-trimethylbenzene, for which a kinetic model was proposed and the system of differential equations was solved.⁵ In the present work we apply that new model of formation of two adducts (triexponential model) to the kinetic data previously¹³ obtained on p-cymene by the flash photolysis-resonance fluorescence (FP-RF) technique over the temperature range between 297 and 350 K in helium buffer gas and perform theoretical calculations in order to identify the adducts, their energies and transition states.

2. Experimental

The experimental setup used in this work has been described elsewhere.^{5, 13-15} Briefly, OH radicals were generated by flash photolysis of water vapour using a Perkin Elmer FX 1165 short arc xenon flash lamp as photolytic light source at an energy of 540 mJ per flash. A quartz resonance lamp was mounted at right angles to the VUV photolysis beam and to the photomultiplier. A gas mixture of $\text{H}_2\text{O}/\text{He}$ was allowed to flow through the resonance lamp. The electrodeless microwave discharge dissociated H_2O to produce electronically excited OH ($\text{A}^2\Pi$). The radiation leaving the lamp was focused into the observation zone exciting the photolytically produced OH radicals in the reaction cell.

Table 1 Experimental conditions. Total pressure 203 ± 2 mbar of helium.

Set #	T and ΔT / K		N ^a	[p-cymene] (min., max.) / 10^{12} cm^{-3}	
1	299.0	0.2	28	5.1	38.8
2	314.6	0.5	43	4.9	39.2
3	316.8	0.5	15	7.0	42.1
4	324.1	0.3	22	7.6	43.4
5	325.9	0.2	36	7.0	42.2
6	326.0	1.8	9	6.7	16.4
7	327.3	0.0	12	7.5	19.8
8	328.5	0.0	57	7.1	42.9
9	329.9	0.2	22	7.3	42.4
10	332.0	0.2	58	6.9	42.6
11	334.2	0.3	21	4.8	39.6
12	334.3	0.2	20	7.2	32.3
13	335.3	0.2	20	6.7	42.1
14	335.7	0.2	26	6.6	39.8
15	336.2	0.0	66	7.1	42.7
16	339.9	1.0	38	5.8	41.6
17	343.5	0.2	18	6.9	41.7
18	345.2	0.1	23	7.3	42.3
19	348.0	0.4	19	7.4	41.7
20	348.9	0.1	45	4.8	39.3

^a number of measurements.

The fluorescence from the reaction cell passed through a 308 nm interference filter and was focused onto the photocathode of a photomultiplier tube (Thorn-EMI, 9789QB). The signal was processed and accumulated using the photon-counting technique with a discriminator and a multichannel scaler board (EG&G Ortec, model ACE MCS) at a dwell time of 0.98 ms, corresponding to a total of 4 s observation time after the flash. The concentration of water vapour in the reaction cell was kept constant at $1.5 \times 10^{15} \text{ cm}^{-3}$, leading to an estimated initial OH radical concentration of $2 \times 10^{10} \text{ cm}^{-3}$.^{16, 17} The p-cymene concentration was varied between $5 \times 10^{12} \text{ cm}^{-3}$ and $55 \times 10^{12} \text{ cm}^{-3}$, which is high enough to assure pseudo first order conditions for OH. In contrast to our previous work¹³, only experiments performed with the xenon flash lamp were used as the set made with the N₂ spark discharge lamp seemed to be affected by impurities increasing the reactivity towards OH. The experimental conditions are summarized in table 1. Differences between this table and table 1 of the preceding part arise because some curves were removed from the biexponential fits. These curves were assumed to be deficient when the intensity ratio and lifetime of the first decay did not increase with increasing p-cymene concentration. The results presented in this work were obtained from all measurements as fits to individual decays were found to be difficult to perform at some combinations of temperature and p-cymene concentrations.

The gases used in this work had the following stated minimum purities: He (Rießner) – 99.996 % ; N₂ (Linde) – 99.999 %. Liquid p-cymene (Aldrich) had a stated minimum purity of 99%. Deionized water was doubly distilled by a quartz still.

3. Theoretical approach

The reaction of OH with p-cymene (PC) is complex due to the presence of two alkyl chains, isopropyl and methyl, which differentiates each site of the molecule with respect to OH attack. The aim of the theoretical calculations is to shed some light into this complex mechanism and help to interpret the experimental results by presenting a comprehensive theoretical investigation of the OH attack on p-cymene. No theoretical investigation of this type has been reported so far on this system.

3.1 Computational details

All calculations were performed using the GAUSSIAN 09 package.¹⁸ The geometries and energies were optimized using density functional theory (DFT) with the hybrid meta exchange-correlation functional M06-2X,¹⁹ coupled to the split valence basis set 6-31G(d,p). This highly nonlocal M06-2X functional developed by Zhao and Truhlar¹⁹ is well suited for structures and energetics, specifically for the determination of energy barriers. The unrestricted Hartree-Fock (UHF) formulation has been used since it is a convenient way to describe open-shell and bond-breaking processes. Its use is justified in our study because we did not observe any significant spin contamination for all the stationary points explored, the quantum average value $\langle S^2 \rangle$ of the square of the total spin operator remaining close to 0.75, i.e., the characteristic value for a doublet state. Full geometry optimization has been performed throughout. We have checked

carefully that all the saddle points found are correctly connected to two minima and are characterized by the existence of only one negative eigenvalue of the Hessian matrix corresponding to an imaginary frequency in the normal-mode analysis.

Since one of our goals is the determination of branching ratios of all the reactive channels, Transition State Theory (TST) is a convenient tool to determine rate constants. In terms of activation free energy ΔG^\ddagger , TST formula reads:

$$k_T \propto g \left(\frac{k_b T}{h} \right) \exp \left[\frac{-\Delta G^\ddagger}{RT} \right] \quad (1)$$

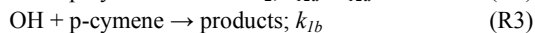
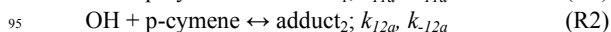
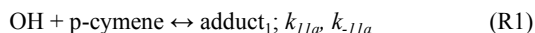
where k_b and h are respectively the Boltzmann and Planck constants and g is the number of equivalent carbon atom sites. Our aim in these calculations is not to obtain absolute values for the rate constants, but rather to look at the relative reactivity of each carbon atom site with respect to OH.

4. Experimental results and discussion

4.1 Kinetic analysis and data evaluation

As outlined above the reversible addition of OH radicals to the aromatic ring in p-cymene can occur at four different positions, leading to the formation of adducts with potentially different properties. The decay curves of OH can deliver first hints about the quantity of distinguishable adducts formed. The initial fast decay corresponds to the consumption of OH radicals by H-atom abstraction and OH addition, while the subsequent slower OH decays are caused by regeneration of OH by a unimolecular decomposition of unstable adducts. A biexponential OH decay indicates the formation of only one adduct or the formation of several adducts with similar kinetic properties, whereas a triexponential OH decay indicates the formation of at least two distinguishable adducts.

Decays curves of OH in the presence of p-cymene were found to be mostly biexponential at temperatures below around 320 K and at temperatures above about 350 K (fig. 1).¹³ In the intermediate range deviations from biexponential behaviour were observed, and the following mechanism for the formation of two adduct species that results in triexponential decay curves was applied to fit the decay curves:⁵



The rate equations that describe the change in the concentrations of OH radicals and of the adducts are shown below.

Cite this: DOI: 10.1039/c0xx00000x

www.rsc.org/pccp

PAPER

Table 2 Rate constants fitted for the p-cymene + OH reaction system (reactions R1-R6).

Set #	k_2 / s ⁻¹	$k_{11a}+k_{12a}+k_{1b}$ /10 ⁻¹² cm ³ s ⁻¹	$k_{11a} k_{-11a}$ /10 ⁻¹² cm ³ s ⁻²	$k_{-11a}+k_{31}$ / s ⁻¹	$k_{12a} k_{-12a}$ /10 ⁻¹² cm ³ s ⁻²	$k_{-12a}+k_{32}$ / s ⁻¹
1	-9.9 ± 4.5	14.9 ± 0.9	81 ± 18 21	24 ± 18 2	13 ± 25 10	6 ± 0.2
2	2.3 ± 2.1	13.1 ± 0.8	303 ± 45 40	52 ± 8 6	11 ± 6 4	7.1 ± 2.3 1.4
3	12.9 ± 1.9	12.7 ± 0.5	310 ± 26 24	61 ± 5	18 ± 5 4	10.3 ± 1.5
4	5.7 ± 2.1	12 ± 0.7	443 ± 56 51	85 ± 7	15 ± 3	10.4 ± 1.3 1.2
5	8.3 ± 1.8	11.9 ± 0.5	496 ± 52 48	92 ± 7 5	15 ± 3	11 ± 1.4 1.1
6	5.4 ± 4.4	14.7 ± 2.9 2.4	919 ± 56 36	107 ± 26 20	17 ± 10 6	10.2 ± 3.2 2.5
7	6.5 ± 2.1 2	11.5 ± 0.7	513 ± 88 77	99 ± 10	15 ± 3	11.4 ± 1.4 1.3
8	7 ± 1.4	11.8 ± 0.5	598 ± 62 57	109 ± 7	17 ± 3 2	12.2 ± 1 0.9
9	6.2 ± 0.1	11.7 ± 0.7	684 ± 102 78	123 ± 10	18 ± 3	13.1 ± 1.4 1.3
10	6.3 ± 1.2	11.7 ± 0.7	791 ± 100 104	141 ± 12 11	18 ± 2	13.9 ± 1.1
11	0.1 ± 1.6 0.1	12.4 ± 2.1 1.6	1255 ± 25	189 ± 32 28	19 ± 7 5	16.1 ± 3.1 2.4
12	12.1 ± 1.8	10 ± 1	713 ± 74 154	152 ± 23 20	26 ± 7 6	20.3 ± 2.6 2.7
13	2.1 ± 1.3	13 ± 1.3 1.2	1387 ± 28	209 ± 22 20	28 ± 4	18.8 ± 1.6 1.5
14	6.8 ± 2.4 2.6	13.1 ± 0.5 2.2	1541 ± 31	203 ± 45 34	29 ± 11 8	19.2 ± 3.7 2.9
15	4.1 ± 1.1	11.7 ± 0.7	1089 ± 22 144	186 ± 15 14	21 ± 3 2	16.8 ± 1.4 1.3
16	4.9 ± 1.7	11.1 ± 1.6 1.5	1450 ± 29	241 ± 36 32	27 ± 8 6	22.5 ± 3.4 3.0
17	0.8 ± 2.1 0.8	11.3 ± 2.5 2.1	1854 ± 37	309 ± 75 62	35 ± 14 11	29.8 ± 5.8 5.5
18	0.1 ± 2.5 0.1	12.6 ± 3.4 2.5	2520 ± 50	354 ± 86 76	35 ± 14 10	30.6 ± 6.0 5.1
19	-1.3 ± 4.8 1.3	16.2 ± 6.9 4.9	4860 ± 2500 970	486 ± 155 127	46 ± 27 18	36.7 ± 8.9 7.9
20	-1.6 ± 3.9 1.6	10.6 ± 10.2 4.4	1847 ± 40	360 ± 480 230	35 ± 59 8	34.3 ± 19.4

10

5

15

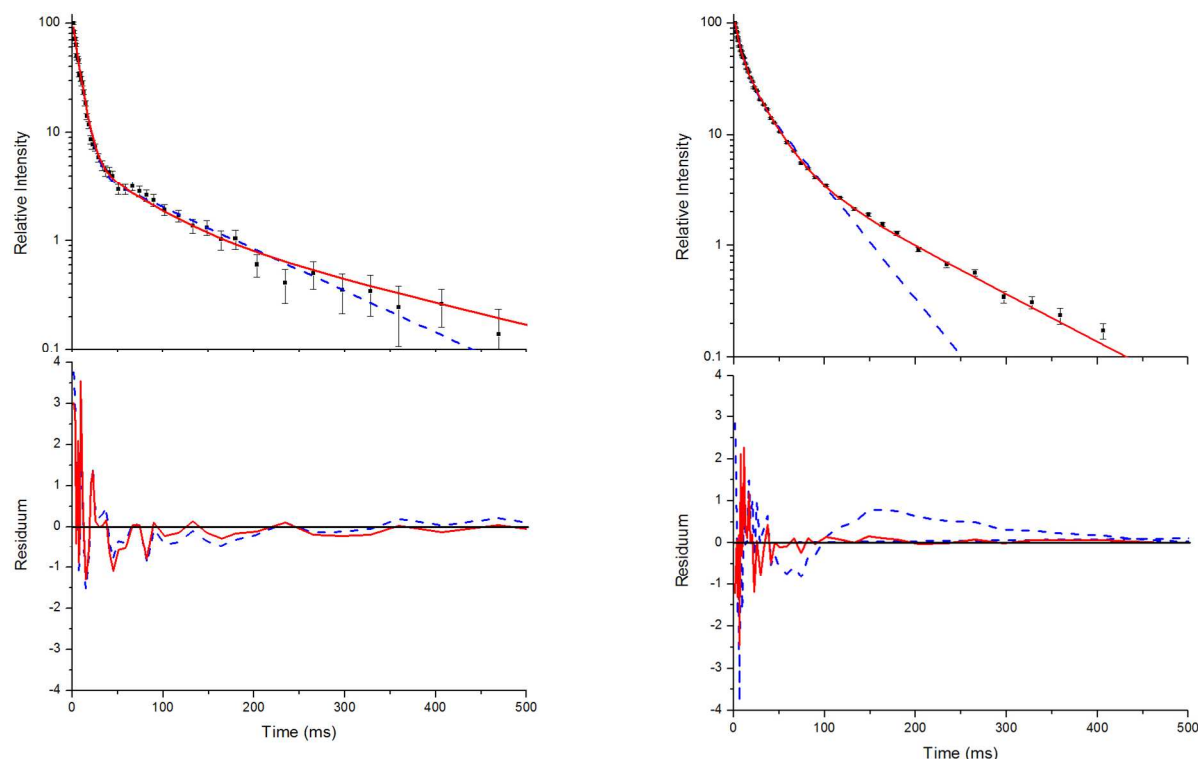


Fig. 1 Typical decay curves of OH (background subtracted), biexponential (blue dashed line) and triexponential (red solid line) model curves and fit residuals for measurements at 299 K (left side) and 330 K (right side) at a p-cymene concentration of $9 \times 10^{12} \text{ cm}^{-3}$ from simultaneous fits to a number (28 and 20 for the left and right side, respectively) of such curves at various concentrations. Obviously, the biexponential model curve satisfactorily describes the data at 299 K but not at 330 K while the triexponential model curves are applicable at both temperatures in agreement with the reaction model considering two adduct species (R1-R6).

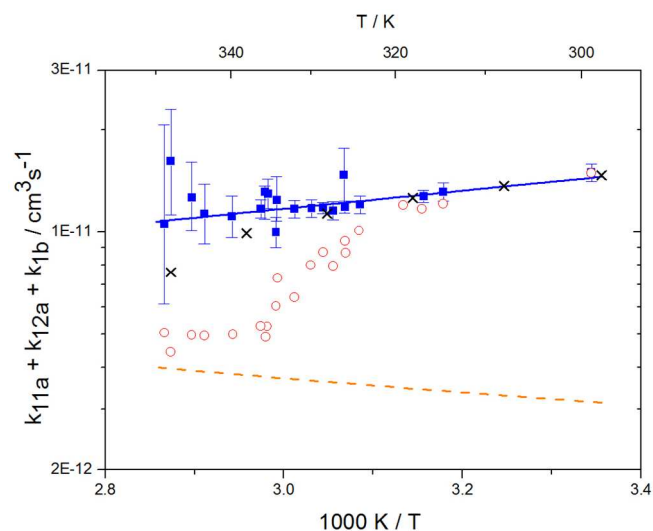


Fig. 2 Arrhenius plot of the total rate constant ($k_{11a} + k_{12a} + k_{1b}$) for the reaction OH + p-cymene. The blue solid line shows the Arrhenius curve for the total rate constants from the triexponential model (blue squares). Red open circles show the results of the biexponential model.¹³ The orange dashed line shows the estimated H-atom abstraction for p-cymene.¹³ Exes show simulated results from a combined theoretical/experimental approach (section 6).

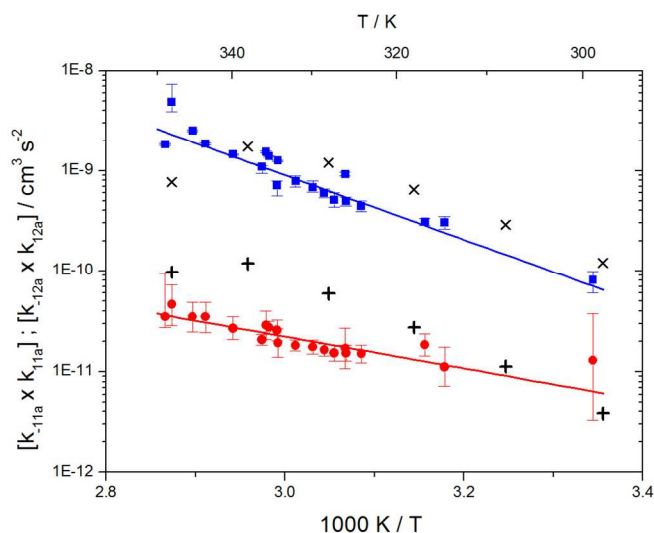


Fig. 3 Arrhenius plot for the product of the forward and backward reaction rate constants for the formation of adduct 1 (blue squares) and adduct 2 (red circles). Solid blue and red lines represent the Arrhenius curves for adduct 1 and 2, respectively. Exes and crosses show simulated results from a combined theoretical/experimental approach (section 6) for adduct 1 and 2, respectively.

$$\frac{d}{dt}[\text{OH}] = -a[\text{OH}] + b[\text{adduct}_1] + e[\text{adduct}_2] \quad (2)$$

$$\frac{d}{dt}[\text{adduct}_1] = c[\text{OH}] - d[\text{adduct}_1] \quad (3)$$

$$\frac{d}{dt}[\text{adduct}_2] = f[\text{OH}] - g[\text{adduct}_2] \quad (4)$$

The combined first-order rate constants are given by:

$$a = k_2 + (k_{11a} + k_{12a} + k_{1b})[\text{p-cymene}] \quad (5)$$

$$b = k_{-11a} \quad (6)$$

$$c = k_{11a}[\text{p-cymene}] \quad (7)$$

$$d = k_{-11a} + k_{31} \quad (8)$$

$$e = k_{-12a} \quad (9)$$

$$f = k_{12a}[\text{p-cymene}] \quad (10)$$

$$g = k_{-12a} + k_{32} \quad (11)$$

Bohn and Zetzsch⁵ proposed the mechanism shown above (R1-R6) for the reaction of the trimethylbenzenes with OH radicals and obtained the analytical solution of the corresponding system of differential equations. This solution allows us to determine the parameters a , b , c , d , e , f , and g for a set of measurements at a given temperature and total pressure. Details on the analytical solution and its limitations in terms of separable parameters are given elsewhere.⁵ Although up to four different adducts can be formed in the OH reaction studied here, we confined our reaction model

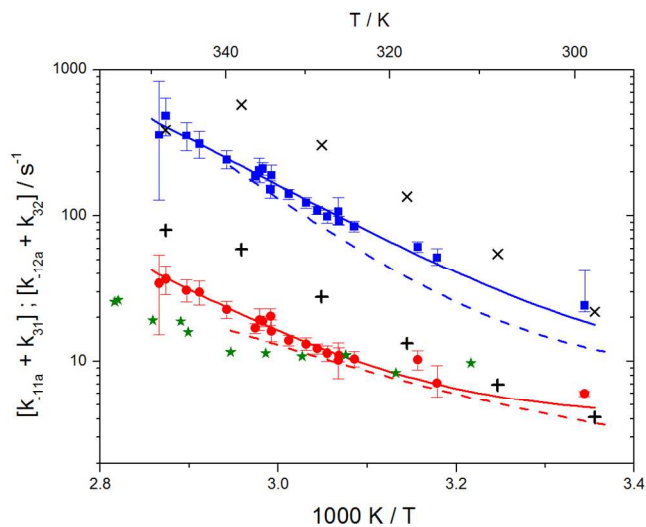


Fig. 4 Arrhenius plot for the sum of unimolecular and background loss rate constants for adduct 1 (blue squares) and adduct 2 (red circles), the hexamethylbenzene adduct (green asterisks).¹⁶ The blue and red dashed lines show the rate constants of the ortho and ipso adduct of 1,3,5-trimethylbenzene.⁵ Solid lines represent the modified Arrhenius curves for the adduct 1 and 2, respectively. Exes and crosses show simulated results from a combined theoretical/experimental approach (section 6) for adduct 1 and 2, respectively.

4.2 Background losses of OH radicals (k_2)

to two adduct species for two reasons. Firstly, because analytical solutions are not available for a greater number of adducts. Secondly, because the precision of the OH decay curves is too poor to permit a proper distinction of three or even four exponentials (fig. 1).

Independent of the model applied, the approach has further limitations. If the decay time of the first exponential decay approaches the time resolution of our experiment (0.98 ms) fit results become distorted. Another limit is reached when the intensity ratio of the first and the second or third decay becomes too small. Then a small and quickly vanishing contribution of the first exponential remains, turning the decays into apparently bi- or monoexponentials. In this work, these limits were reached at temperatures larger than about 350 K and therefore higher temperatures were not considered.

Technical details on the fitting procedure and on the estimation of parameter uncertainties can be found elsewhere.^{5, 13} Error estimates for the exponential term in the Arrhenius and van't Hoff expressions were obtained by fitting the maximum and minimum parameter values, respectively. Due to the small temperature range, errors in the pre-exponential factors were large and therefore will not be presented here. Table 2 summarizes the combined rate constants for each isothermal set of measurements.

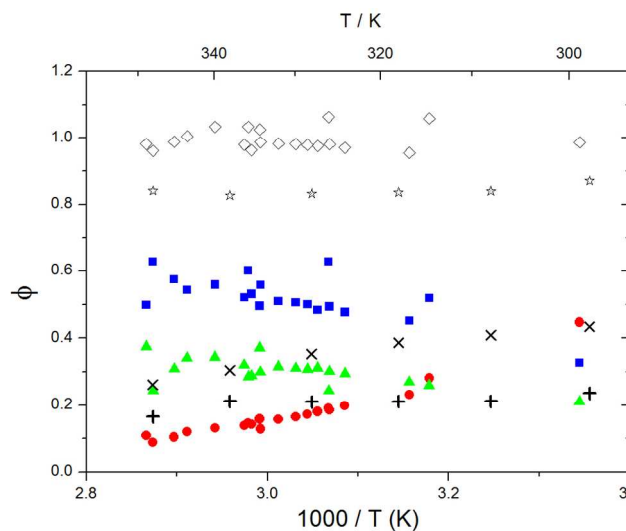


Fig. 5. Formation yields for adduct 1 (blue squares), adduct 2 (red circles) and H-atom abstraction (green triangles) after optimization of k_{31} and k_{32} . Rhombi show the sum of the calculated yields. Exes, crosses and stars show simulated results of a combined theoretical/experimental approach (section 6) for adduct 1 and 2, and their sum, respectively.

OH radicals may also react with minor impurities that can enter the cell from the dosing system (previous or present sample), the carrier gas or from wall desorption and leaks. Diffusion of OH radicals from the observation zone due to concentration gradient between the irradiated volume and the cell walls as well as transport due to the constant gas flow may

contribute to the OH radical losses described by the rate constant k_2 . This rate constant comprised several processes, and therefore its complete understanding is complicated and related to the experimental conditions applied. In this work, the average loss rate constant was found to be 4 s^{-1} in good agreement with the experimental lifetime of OH radicals in our system without any reactant of about 3 s^{-1} . In contrast to the previous paper, applying the triexponential model to our measurements, some k_2 values were negative. This irregularity was found to have no effect on the determination of other combined rate constants, corroborated by the good agreement with other constants determined at similar temperatures.

4.3 OH + p-cymene ($k_{OH} = k_{11a} + k_{12a} + k_{1b}$)

Analogous to the biexponential model, the fitting procedure allows us to determine the total rate constant for the reaction between OH radicals and p-cymene, but not each rate constant individually. In the case of the triexponential model, the total rate constant consists of three rate constants: OH addition for the formation of adducts 1 (k_{11a}) and 2 (k_{12a}), and H-atom abstraction (k_{1b}). The total rate constant was found to be $(14.9 \pm 0.9) \times 10^{-12} \text{ cm}^3 \text{ s}^{-1}$ at 299 K. This value is in good agreement with the value published by Corchnoy and Atkinson $(15.1 \pm 4.1) \times 10^{-12} \text{ cm}^3 \text{ s}^{-1}$.¹² At temperatures up to around 320 K, biexponential¹³ and triexponential models show good agreement, but deviating results at higher temperatures where the fit quality for the biexponential model was also poor (fig. 2). This behaviour was also observed for 1,3,5-trimethylbenzene,⁵ an aromatic compound which can react with OH radicals to form two different adducts alone. The Arrhenius expression for the total rate constant was determined as $k_{OH} = 1.9 \times 10^{-12} \exp(610 \pm 210) \text{ K/T cm}^3 \text{ s}^{-1}$, comparable with the previously obtained for temperatures below 320 K.¹³

4.4 Forward and backward reactions (k_{11a} k_{-11a} ; k_{12a} k_{-12a})

The analytical solution of the differential equation system for the triexponential model does not allow us to separate the rate constants for the forward (k_{11a} and k_{12a}) and backward reactions (k_{-11a} and k_{-12a}), but allows us to determine their products ($k_{11a} k_{-11a}$ and $k_{12a} k_{-12a}$).⁵ A semi-logarithmic plot of these products versus the inverse temperature (figure 3) was used to determine the sum of the activation energies for OH addition and unimolecular decay for each of the adducts.

The product of the rate constants for the forward and backward reaction for both adducts increases with increasing temperature. Simple Arrhenius expressions of the form $k = A \exp(-B/T)$ were fitted to the data at temperatures between 299 and 349 K resulting in $k_{11a} k_{-11a} = 4 \exp[(-7400 \pm 550) \text{ K/T}] \text{ cm}^3 \text{ s}^{-2}$ for adduct 1 and $k_{12a} k_{-12a} = 1.2 \times 10^{-6} \exp[(-3620 \pm 1200) \text{ K/T}] \text{ cm}^3 \text{ s}^{-2}$ for adduct 2. The sums of activation energies of forward and backward reactions were calculated from the B parameters to be $(62 \pm 5) \text{ kJ mol}^{-1}$ and $(30 \pm 10) \text{ kJ mol}^{-1}$ for adduct 1 and 2 respectively.

4.5 Unimolecular decay and background loss of the adducts ($k_{-11a} + k_{31}$; $k_{-12a} + k_{32}$) and adduct formation yields

Another combined rate constant that can be directly determined is the sum of the rate constants of unimolecular decay of the adducts back to the reactants and other products and of background losses by reactions with impurities. Possible perturbations by radical-radical reactions and diffusion processes have been already investigated.⁵ While the unimolecular decay of the adducts strongly depends on the temperature, background reactions are assumed to be constant in the studied temperature range. Adduct loss rate constants for each adduct were fitted between 299 and 350 K to a function of the form $k = A \exp(-B/T) + C$. However, in a first step optimized parameters C were determined using expressions for the adduct yields and OH budget considerations.

Adduct formation yields were determined using equations 12-15. The rate constants k_{1b} of H atom abstraction were taken from our previous work¹³: $k_{1b} = 2 \times 10^{-17} (T/\text{K})^2 \exp(170 \text{ K/T}) \text{ cm}^3 \text{ s}^{-1}$. At low temperatures, the denominators ($d - k_{31}$) and ($g - k_{32}$) are getting very small, making the obtained yields strongly dependent on k_{31} and k_{32} . Optimized values (7.5 ± 3.2) and $(4.1 \pm 0.3) \text{ s}^{-1}$ were determined for k_{31} and k_{32} , respectively, that correspond to an average total yield of unity.

$$\Phi_1 = \frac{k_{11a}}{k_{OH}} = \frac{k_{11a} k_{-11a}}{k_{OH} k_{-11a}} = \frac{bc}{k_{OH} (d - k_{31})} \quad (12)$$

$$\Phi_2 = \frac{k_{12a}}{k_{OH}} = \frac{k_{12a} k_{-12a}}{k_{OH} k_{-12a}} = \frac{ef}{k_{OH} (g - k_{32})} \quad (13)$$

$$\Phi_{abst} = \frac{k_{1b}}{k_{OH}} \quad (14)$$

$$\sum \Phi_i = 1 \quad (15)$$

The various yields are shown in figure 5. The yields of adduct 1 and adduct 2 are similar at room temperature but then decrease and increase with temperature, respectively. Expectedly, the total adduct yield decreases with temperature because of an increasing yield of H-atom abstraction. Background loss rate constants were found to be in good agreement with those found in the literature for benzene,^{20, 21} toluene,^{20, 21} p-xylene,²² 1,3,5-TMB⁵ and hexamethylbenzene,¹⁶ ranging from 2 to 8 s^{-1} . Using the optimized values of k_{31} and k_{32} , Arrhenius expressions for the rate constants of unimolecular decompositions of the adducts were obtained: $k_{-11a} = 1 \times 10^{12} \exp[(-7620 \pm 840) \text{ K/T}] \text{ s}^{-1}$ and $k_{-12a} = 3 \times 10^{11} \exp[(-8020 \pm 260) \text{ K/T}] \text{ s}^{-1}$.

Activation energies for both adducts are very similar with values of 60 ± 7 and $67 \pm 2 \text{ kJ mol}^{-1}$ for adduct 1 and 2, respectively. These are rather similar to adducts formed from the OH radical addition to a non-occupied position as in the case of benzene (72 kJ mol^{-1}).²⁰ Figure 4 shows the adduct loss rate constants for both p-cymene adducts in comparison with

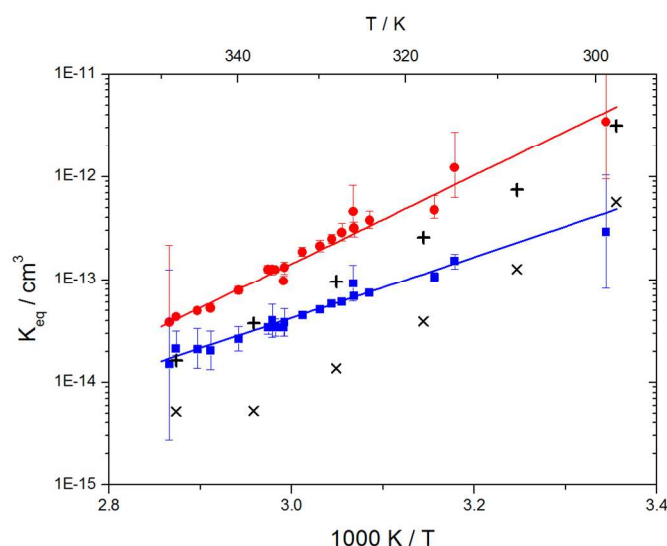


Fig. 6 Equilibrium constants for adduct 1 (blue squares) and adduct 2 (red circles). Solid lines represent the regression curves between 299 and 345 K (equations 18 and 19). Exes and crosses show the simulated results from a combined theoretical/ experimental approach (section 6) for adduct 1 and 2, respectively.

hexamethylbenzene¹⁶ and both mesitylene⁵ adducts. The dissociation rate constants found for the p-cymene adducts are very similar to the ones corresponding to the mesitylene adducts where only two isomers, ipso and ortho, can be formed. Furthermore, adducts 2 of p-cymene and mesitylene have low dissociation rate constants that are comparable to those obtained for hexamethylbenzene¹⁶ where only ipso adducts are possible. The similarity of the activation energies of the adducts with the one of benzene, as well as the similarity of the dissociation rate constants of adduct 2 with the ones published for hexamethylbenzene make it very difficult to identify which adduct or group of adducts is responsible for the triexponential OH decays observed.

4.6 Equilibrium constants (K_{eq1} , K_{eq2}) and thermochemical data

A measure of the stability of the adducts is given by their equilibrium constants, K_{eq1} , K_{eq2} (fig 6). These constants were estimated using equation 16 and 17 with background losses (k_{31} and k_{32}) determined in the previous section.

$$K_{eq1} = \frac{bc}{[d-k_{31}]^2} \quad (16)$$

$$K_{eq2} = \frac{ef}{[g-k_{32}]^2} \quad (17)$$

Equilibrium constants for both adducts are shown in fig. 5 and can be expressed between 299 and 345 K by following equations:

$$K_{eq1} = 6.2 \times 10^{-26} (T/K) \exp [(7150 \pm 170) K/T] \text{ cm}^3 \quad (18)$$

$$K_{eq2} = 2.3 \times 10^{-29} (T/K) \exp [(10200 \pm 1200) K/T] \text{ cm}^3 \quad (19)$$

Standard reaction enthalpies and entropies were determined for each adduct using a van't Hoff expression (20). The values

obtained were: $\Delta H_1 = (-59 \pm 1) \text{ kJ mol}^{-1}$, $\Delta S_1 = (-64 \pm 6) \text{ J mol}^{-1} \text{ K}^{-1}$ for the first and $\Delta H_2 = (-85 \pm 10) \text{ kJ mol}^{-1}$, $\Delta S_2 = (-130 \pm 27) \text{ J mol}^{-1} \text{ K}^{-1}$ for the second adduct.

$$K_{eq} = \frac{k_b T}{p^\theta} \exp\left(-\frac{\Delta H}{RT} + \frac{\Delta S}{R}\right) \quad (20)$$

The reaction enthalpy of adduct 2 is in reasonable agreement with results for other OH aromatics adducts from the literature.²³ However, the reaction enthalpy of adduct 1 is significantly smaller which is also in contradiction with theoretical predictions for different adduct isomers from other aromatics.²⁴⁻²⁸ Moreover, the reaction entropy of adduct 1 is clearly too small for an association reaction and should in any case be very similar for both adducts. These inconsistencies point towards a perturbation possibly caused by the presence of more than two adduct species. In our previous work,¹³ the reduced χ^2 was applied to reject the simpler model for the formation of one single adduct. The mechanism proposed in the present work strongly improves the fit quality. However, despite the huge improvements reached by the triexponential model, there are still some high χ^2 values at temperatures between 330 and 340 K. These values might indicate the influence of further adduct species producing a departure from triexponential decays. To evaluate these deviations, OH decay curves with much higher precision would be needed as well as numerical tools to fit these curves but this is beyond our current capabilities.

5. Theoretical results

5.1 OH addition to p-cymene

As shown in scheme 1, OH radical addition to the aromatic ring of p-cymene may form four isomers of p-cymene-OH adducts, two ipso isomers ($\text{PC}_{\text{ipso}}\text{-CH}_3$ and $\text{PC}_{\text{ipso}}\text{-C}_3\text{H}_7$) and two ortho isomers ($\text{PC}_{\text{ortho}}\text{-CH}_3$ or $\text{PC}_{\text{ortho}}\text{-C}_3\text{H}_7$). The correlation diagram between the relevant stationary states is illustrated in figure 7, and the corresponding zero-point corrected energies are gathered in Table 3. The pathways are initiated by the formation of the pre-reactive complex (PRC in figure 7) typical of electrophilic addition to aromatics²⁹ which corresponds to a long range interaction between p-cymene and the OH radical and is common to each addition channel. In this structure, the radical OH is situated above the aromatic ring. This PRC lies 26 kJ mol^{-1} below the energy of the separated reactants. On the way from the PRC to TS_{add} , the C-O distance diminishes from 2.5 \AA to $\sim 2.0 \text{ \AA}$. It can be seen that the reactions are all exothermic by -85 kJ mol^{-1} in a narrow range of 5 kJ mol^{-1} . The $\Delta E_0^\#$ barriers, called TS_{add} in a generic way, are also very close together in a range between -2.4 and $+2.5 \text{ kJ mol}^{-1}$. Such small values could suggest that the yields of ipso and ortho adducts are similar. In fact, the entropy change from the reactants to the TS is no more negligible and its value can be different from one pathway to the other. It is therefore essential to take into account the change of entropy in each pathway by calculating the Gibbs free energy barriers $\Delta G_T^\# = \Delta H_T^\# - T\Delta S_T^\#$ at temperature T. On the basis of the calculated $\Delta G_{298}^\#$ values, bimolecular OH-addition rate constants were calculated from equation 1. The branching ratios ρ_{add} are easily determined from the ratio of each rate constant channel over the total rate constant. All these data is collected in Table 3.

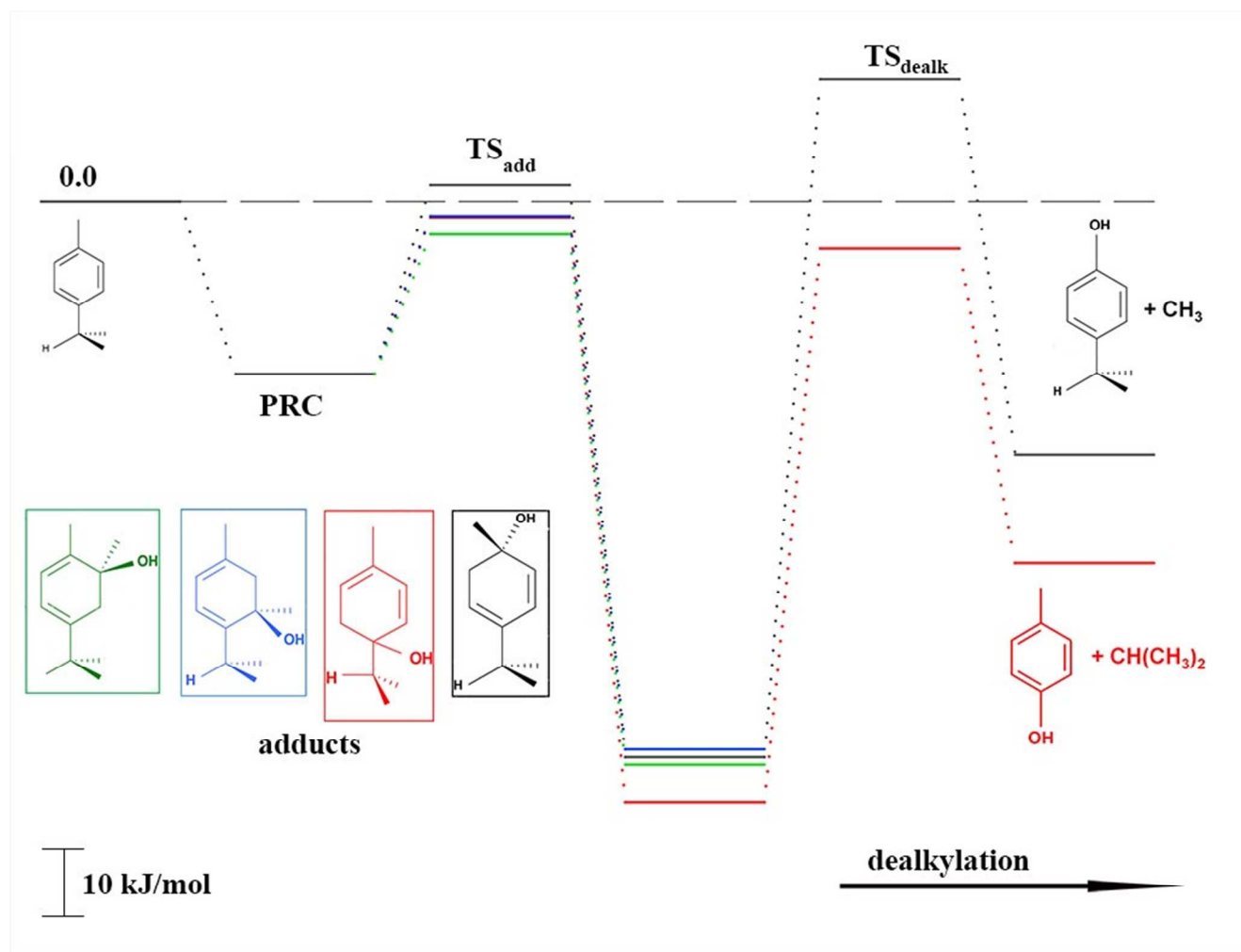


Fig.7 Energy diagram for the addition reaction p-cymene + OH and successive dealkylation of the ipso adducts.

As a result of our calculations, it can be predicted that, among the four different addition possibilities: i) the formation of the ipso-CH₃ adduct can be neglected from the reaction mechanism (3% of the total addition); ii) the formation of ortho adducts is predominant (79%); iii) the ipso-C₃H₇ adduct is formed (by 18% of total addition) but can further dissociate, via dealkylation, to give new products. This is the subject of the following section.

5.2 Formation of cresol by dealkylation of ipso adducts

PC_{ipso}-C₃H₇ and PC_{ipso}-CH₃ may dealkylate to form the phenol type compounds p-cresol + isopropyl radical (C₃H₇) and 4-isopropyl phenol + methyl radical (CH₃). The calculated transition state and reaction energies for both of these decompositions are sketched in the right part of figure 7. The overall reaction energies OH + p-cymene, leading to the formation of 4-isopropyl phenol + CH₃ or p-cresol + C₃H₇, are

exothermic by -38 kJ mol^{-1} and -52 kJ mol^{-1} .

The corresponding free energies of activation, $\Delta G_{298}^{\ddagger}$ for 298 K, suggest that only the isopropyl departure from the ipso-C₃H₇ adduct can occur at room temperature, since the energy barrier is lower by -7 kJ mol^{-1} than the energy of the reactants p-cymene + OH. In order to test this assumption, we have performed some preliminary kinetic calculations on this dealkylation channel by using a statistical approach based on a RRKM-like³⁰ methodology. Based on the potential energy profile obtained from DFT calculations, data presented in table 3 was used for the kinetic analysis. For each of these stationary points, harmonic vibrational wavenumbers and the rotational constants calculated by the GAUSSIAN09 quantum chemistry program¹⁸ were used. Table 4 summarizes these results at two temperatures and two pressures.

Cite this: DOI: 10.1039/c0xx00000x

www.rsc.org/pccp

PAPER

Table 3 M06-2X/6-31G(d,p) Zero-point corrected energy barriers (ZPE), $\Delta E_0^\#$, activation enthalpies $\Delta H_{298}^\#$, activation entropies $\Delta S_{298}^\#$, free energy barriers, $\Delta G_{298}^\#$, and reaction energies, relative to the reactants p-cymene + OH^a, and branching ratios, ρ_{add} (i.e. the percentage of each addition site). The ZPE barrier for dealkylation $\Delta E_0^\#(TS_{dealk})$ and energy for cresol formation, ΔE_0 (cresol formation). The energy of the Pre-Reactive Complex, $\Delta E_0(PCR)$, is $-25.9 \text{ kJ mol}^{-1}$.

	$\Delta E_0^\#$	$\Delta H_{298}^\#$	$\Delta S_{298}^\#$	$\Delta G_{298}^\#$	ΔE_0 Adduct	ρ_{add} (%)	$\Delta E_0^\#$ TS _{dealk}	ΔE_0 Cresol formation
PC _{ipso} -CH ₃	2.5	-1.9	-149.8	42.7	-83.6	3	18.4	-38.1
PC _{ipso} -C ₃ H ₇	-2.4	-6.6	-151.3	38.5	-90.3	18	-7.1	-52.3
PC _{ortho} -CH ₃	-0.8	-5.1	-149.5	39.5	-84.7	24		
PC _{ortho} -C ₃ H ₇	-2.2	-6.2	-146.3	37.4	-82.4	55		

^a Energies are given in kJ mol^{-1} . ^b Entropies in $\text{J mol}^{-1} \text{ K}^{-1}$.

Table 4 Kinetic calculations on the dealkylation channel from the ipso-C₃H₇ adduct.

T/K	P/mbar	k_{loss} / $10^{-13} \text{ cm}^3 \text{ s}^{-1}$	k_{prod} / $10^{-18} \text{ cm}^3 \text{ s}^{-1}$	k_{adduct} / $10^{-13} \text{ cm}^3 \text{ s}^{-1}$	β
298	760	0.166	6.18	0.166	0.05
400	760	0.194	116	0.193	0.1
298	380	0.166	12.3	0.166	0.05

^a k_{loss} : disappearance of the reactants for this addition channel; k_{prod} : immediate formation of products p-cresol + C₃H₇; k_{adduct} : stabilization of the ipso adduct; β : rate of regeneration of the reactants OH and p-cymene from the adduct divided by the formation of products p-cresol + C₃H₇ from the adduct

Table 5 Calculated M06-2X/6-31G(d,p) reaction entropies^a ΔS_{298} , reaction enthalpies, ΔH_{298} , reaction free energies, ΔG_{298} at 298 K (relative to the reactants p-cymene + OH^b) and calculated equilibrium constants, $K_{eq}(T) = k_B T / p^\circ \exp[-\Delta G_{298} / RT]$ for the four theoretically possible adducts and experimental results for comparison.

	ΔS_{298}^a	ΔH_{298}^b	ΔG_{298}^b	$K_{eq}(298 \text{ K})^c$ / 10^{-13}
PC _{ipso} -CH ₃	-161.1	-89.2	-41.2	7.0
PC _{ipso} -C ₃ H ₇	-155.2	-95.3	-49.0	160
PC _{ortho} -CH ₃	-154.0	-89.6	-43.7	19
PC _{ortho} -C ₃ H ₇	-163.2	-87.9	-39.3	3.2
Adduct 1 ^d	-64 ± 6	-59 ± 1	-40 ± 1	4.9
Adduct 2 ^d	-130 ± 27	-85 ± 10	-46 ± 2	50

^a Entropies in $\text{J mol}^{-1} \text{ K}^{-1}$, ^b energies in kJ mol^{-1} , ^c K_{eq} in cm^3 , ^d this work (experimental)

While there is no significant direct formation of cresol from OH + cymene, cresol is the main product of the unimolecular decomposition of the stabilized PC_{ipso}-C₃H₇ as indicated by the factor β . This finding is not in contradiction with product studies

that showed no significant (<2%) cresol formation¹¹ because in the presence of O₂ cresol formation competes with the PC_{ipso}-C₃H₇ + O₂ reaction that is expected to be much faster under atmospheric conditions. However, in the absence of O₂,

confirmation of cresol formation would be a strong indicator for the presence of the ipso adduct.

5.3 Results for reaction entropies, enthalpies and equilibrium constants

Reaction entropies ΔS_{298} , reaction enthalpies ΔH_{298} and equilibrium constants K_{eq} have been calculated for the addition reactions at 298 K and are collected in Table 5, together with the corresponding experimental results obtained in this work. Calculated enthalpies are in good agreement with literature data for different OH adduct isomers from other aromatics.²³⁻²⁸ As the ipso-CH₃ contribution is minor, and the ipso-C₃H₇ is expected to mainly dealkylate to cresol, the two adducts that are theoretically expected to determine OH regeneration are the remaining ortho-CH₃ and ortho-C₃H₇ adducts. Experimental entropy and enthalpy changes for adduct 1 are much smaller than those obtained from DFT calculations. This disagreement might arise from a wrongful application of the triexponential model to a system with three or four adducts, as mentioned in Sect. 4.6. Even though the obtained experimental enthalpy and entropy for adduct 2 are more comparable with the theoretical values, the experimental uncertainty does not allow to clearly identify this adduct. Nevertheless, the lower yields and greater equilibrium constants are closer to the predictions for the ortho-CH₃ adduct. In order to make the theoretical and experimental results more comparable, numerical simulations were performed and will be presented in the following section.

6. Comparison of experimental and theoretical results using simulated OH decays

The theoretical results presented in the previous section predict the formation of all four possible adduct isomers. However, the relative yields and kinetic properties regarding back-decomposition and dealkylation are different for the different isomers. The question arises what results would be obtained from corresponding OH decay curves using the same data analysis that was applied for the experimental data of this work. To answer this question, OH decay curves were simulated by numerical calculations at a similar range of temperatures and reactant concentrations for direct comparison. For this purpose, a complete set of rate constants as a function of temperature is necessary.

We used the TST predicted adduct yields and the measured total rate constants of adduct formation (k_{add}) to make simulations and measurements more comparable. Values of k_{add} were obtained by subtracting the rate constants of abstraction k_{1b} from the k_{OH} obtained in this work:

$$k_{add} = k_{OH} - k_{1b} \quad (21)$$

using the Arrhenius expressions of k_{OH} and k_{1b} given in Sect. 4.3 and 4.5. The total rate constant k_{OH} is considered to be a robust quantity that can be extracted from the experimental data without knowing the actual number of isomers formed. Using Eq. 1 and the ΔH_{298}^\ddagger and ΔS_{298}^\ddagger data (Tab. 3), adduct yields ρ_T were calculated for six temperatures in a range 298-348 K and scaled with the corresponding k_{add} .

$$k_{add}(i) = k_{add} \times \rho(i) \quad (22)$$

Here i stands for the different isomers and the resulting individual rate constants $k_{add}(i)$ are listed in Tab. 6. It should be noted that the temperature dependencies of enthalpies and entropies are negligible (<1%) in the narrow range considered here. In a second step, the first-order rate constants of adduct dissociation back to OH + *p*-cymene, $k_{cym}(i)$ were determined from the equilibrium constants K_{eq} obtained from the theoretically calculated ΔH_{298} and ΔS_{298} of the adduct formation reactions (Tab. 5).

$$k_{cym}(i) = k_{add}(i) / K_{eq}(i) \quad (23)$$

For the PC_{ipso}-C₃H₇ isomer also the rate constants of cresol formation were calculated from the estimated ratios β of rate constants of back-dissociation and cresol formation for this isomer (table 4).

$$k_{cresol}(PC_{ipso} - C_3H_7) = k_{cym}(PC_{ipso} - C_3H_7) / \beta \quad (24)$$

In Tab. 7 the obtained first-order rate constants $k_{cresol}(PC_{ipso} - C_3H_7)$ and the $k_{cym}(i)$ for all isomers are listed. The rate constants in Tab. 6 and 7 reveal that theoretically only a slight variation of adduct yields with temperature is expected. Moreover, the yield of PC_{ipso}-CH₃ remains below 5% at all temperatures and the predicted main fate of PC_{ipso}-C₃H₇ is decomposition to cresol + C₃H₇.

Based on the rate constants in Tab. 6 and 7, OH decay curves were simulated numerically using FACSIMILE (MCPA Software Ltd., Oxfordshire, UK) assuming a realistic OH starting concentration of $1 \times 10^{10} \text{ cm}^{-3}$. Additional background loss rate constants of 3 s^{-1} for all adduct isomers and 10 s^{-1} for OH were also implemented to improve the comparability with experimental conditions. Decay curves were produced for five *p*-cymene concentrations in the range $0.8\text{--}4 \times 10^{13} \text{ cm}^{-3}$ as in the real experiments for the six temperatures under consideration. The obtained concentration profiles were then converted to count rates including background and finally to count numbers binned exactly as in the real experiments. Poisson random noise was added dependent on the count numbers and 150 single OH decay curves were accumulated to simulate the typical repetition of single shot experiments.

For each temperature simultaneous fits to the five decay curves at different *p*-cymene concentrations were then performed with the software tools developed for the experimental data. Fit results varied slightly when the procedure described in the last paragraph was repeated caused by the applied random noise. Experiment simulations and fits were therefore repeated 100 times to obtain mean values and standard deviations of fit parameters and fit qualities. The results are listed in Tab. 8 and shown as black symbols for direct comparison in Figs. 2-6.

Previous applications of the method showed that simulations based on the pure two-adduct model (R1-R6) exactly returned the rate constants used for the numerical calculations. Moreover, in these cases the mean fit quality parameter χ^2/DOF was unity.⁵ This is the expected ideal result when experimental uncertainties

are known as for the simulations. A significant deviation from unity therefore indicates a departure of the mechanism from the two-adduct model. In the case discussed here there is merely a slight deviation which is hardly significant. Thus within the simulated uncertainties OH decay curves are effectively triexponential in agreement with the two-adduct model. The explanation of course is that two of the four adduct isomers that are formed play a minor role because either their yield is low (PC_{ipso}-CH₃) or they mainly decompose to products other than OH (PC_{ipso}-C₃H₇).

While the OH background loss rate constant k_2 is reproduced in all cases, with increasing temperature the fitted k_{OH} tend to deviate from those applied in the simulations (Tab. 6). Note that this deviation is not accompanied by a decrease of fit quality, so there are compensating effects, and fit quality therefore is a necessary but not sufficient condition that a reaction model is

correct. Moreover, in the presence of a fast decomposing adduct the range of useful temperatures for such an analysis is clearly limited as explained in Sec. 4.1. In the simulated measurements this limit is already reached around 340 K as is evident from the levelling off of adduct 1 rate constants at greater temperatures.

Expectedly, the parameters k_{11a} k_{-11a} and k_{12a} k_{-12a} roughly correspond to the products $k_{add}(PC_{ortho}-C_3H_7) \times k_{cym}(PC_{ortho}-C_3H_7)$ and $k_{add}(PC_{ortho}-CH_3) \times k_{cym}(PC_{ortho}-CH_3)$, respectively. And the parameters $k_{-11a}+k_{31}$ and $k_{-12a}+k_{32}$ more or less resemble $k_{cym}(PC_{ortho}-C_3H_7) + 3 \text{ s}^{-1}$ and $k_{cym}(PC_{ortho}-CH_3) + 3 \text{ s}^{-1}$, respectively, but the agreement is not perfect showing that the influence of the two *ipso*-isomers is not completely negligible even at the lowest temperature. Nevertheless, the further analysis reveals that the two adduct approach is also sufficient to extract reasonable values of adduct yields (Fig. 5) and equilibrium constants (Fig. 6) of the two adducts.

Table 6 k_{OH} , k_{1b} and individual rate constants of adduct formation $k_{add(i)}$ of four adduct isomers at different temperatures. The $k_{add(i)}$ were calculated from theoretically predicted isomer yields and the experimental total rate constant of adduct formation $k_{add} = k_{OH} - k_{1b}$

T / K	$k_{OH} / 10^{-11} \text{ cm}^3 \text{ s}^{-1}$	$k_{1b} / 10^{-12} \text{ cm}^3 \text{ s}^{-1}$	$k_{add}(PC_{ipso}-CH_3) / 10^{-12} \text{ cm}^3 \text{ s}^{-1}$	$k_{add}(PC_{ipso}-C_3H_7) / 10^{-12} \text{ cm}^3 \text{ s}^{-1}$	$k_{add}(PC_{ortho}-CH_3) / 10^{-12} \text{ cm}^3 \text{ s}^{-1}$	$k_{add}(PC_{ortho}-C_3H_7) / 10^{-12} \text{ cm}^3 \text{ s}^{-1}$
298.0	1.47	3.14	0.380 (3%)	2.06 (18%)	2.78 (24%)	6.35 (55%)
308.0	1.38	3.29	0.362	1.84	2.54	5.73
318.0	1.29	3.45	0.344	1.65	2.32	5.16
328.0	1.22	3.61	0.326	1.48	2.12	4.66
338.0	1.15	3.78	0.307	1.33	1.93	4.20
348.0	1.10	3.95	0.289 (4%)	1.19 (17%)	1.76 (25%)	3.78 (54%)

Table 7 First-order rate constants of cresol + C₃H₇ formation from the PC_{ipso}-C₃H₇ isomer and individual rate constants of OH + *p*-cymene formation $k_{cym(i)}$ from all four OH adduct isomers at different temperatures. The $k_{cym(i)}$ were calculated from theoretically predicted equilibrium constants and the $k_{add(i)}$ of Tab. 5. The ratios k_{cym}/k_{cresol} correspond to the theoretically predicted β (see Section 5.2)

T / K	$k_{cresol}(PC_{ipso}-C_3H_7) / \text{ s}^{-1}$	$k_{cym}(PC_{ipso}-CH_3) / \text{ s}^{-1}$	$k_{cym}(PC_{ipso}-C_3H_7) / \text{ s}^{-1}$	$k_{cym}(PC_{ortho}-CH_3) / \text{ s}^{-1}$	$k_{cym}(PC_{ortho}-C_3H_7) / \text{ s}^{-1}$
298.0	2.56	0.545	0.128	1.48	19.8
308.0	7.06	1.62	0.387	4.24	54.6
318.0	18.1	4.46	1.08	11.3	141
328.0	43.8	11.5	2.83	28.0	339
338.0	99.5	27.6	6.93	65.6	769
348.0	214	62.7	16.0	145	1650

Table 8 Mean fit results and fit qualities with standard deviations from the analysis of numerically calculated OH decay curves and simulated experiments with random noise. Parameters correspond to those in Tab. 2 but standard deviations were obtained from 100 simulated experiments for each set of OH decay curves.

T / K	$k_2 / \text{ s}^{-1}$	$k_{11a}+k_{12a}+k_{1b} / 10^{-11} \text{ cm}^3 \text{ s}^{-1}$ (= k_{OH})	$k_{11a} k_{-11a} / 10^{-10} \text{ cm}^3 \text{ s}^{-2}$	$k_{12a} k_{-12a} / 10^{-11} \text{ cm}^3 \text{ s}^{-2}$	$k_{-11a}+k_{31} / \text{ s}^{-1}$	$k_{-12a}+k_{32} / \text{ s}^{-1}$	χ^2 / DOF
298.0	9.3 ± 1.1	1.464 ± 0.013	1.20 ± 0.02	0.38 ± 0.10	21.9 ± 0.6	4.1 ± 0.6	1.17 ± 0.10
308.0	8.9 ± 0.8	1.365 ± 0.014	2.91 ± 0.06	1.13 ± 0.07	55.1 ± 0.9	6.9 ± 0.3	1.12 ± 0.09
318.0	9.4 ± 0.7	1.258 ± 0.022	6.44 ± 0.28	2.73 ± 0.11	135.6 ± 3.3	13.3 ± 0.3	1.09 ± 0.09
328.0	10.1 ± 0.6	1.134 ± 0.034	12.0 ± 1.2	5.92 ± 0.21	303 ± 15	27.8 ± 0.6	1.07 ± 0.09
338.0	10.4 ± 0.8	0.996 ± 0.091	17.5 ± 7.1	11.8 ± 0.8	580 ± 110	59.0 ± 1.6	1.05 ± 0.08
348.0	11.2 ± 1.0	0.76 ± 0.11	7.7 ± 8.5	9.7 ± 8.5	390 ± 310	80 ± 38	1.04 ± 0.10

Moreover, the decomposition of the $\text{PC}_{\text{ipso}}\text{-C}_3\text{H}_7$ to cresol can be recognized by the fact that only about 90% of k_{OH} can be accounted for by $k_{11a}+k_{12a}+k_{1b}$. However, no such missing yield was recognized in the experiments that show no evidence for any unaccounted loss of OH.

Regarding the thermodynamic data, reaction enthalpies of -90 kJ mol^{-1} (adduct 1) and -89 kJ mol^{-1} (adduct 2) were obtained considering a temperature range $< 340 \text{ K}$ that compare very well with the data applied to calculate the rate constants: -88 kJ mol^{-1} ($\text{PC}_{\text{ortho}}\text{-C}_3\text{H}_7$) and -90 kJ mol^{-1} ($\text{PC}_{\text{ortho}}\text{-CH}_3$). Reaction entropies are also in good agreement: $-166 \text{ J mol}^{-1} \text{ K}^{-1}$ (adduct 1) and $-146 \text{ J mol}^{-1} \text{ K}^{-1}$ (adduct 2) compared to $-163 \text{ J mol}^{-1} \text{ K}^{-1}$ ($\text{PC}_{\text{ortho}}\text{-C}_3\text{H}_7$) and $-154 \text{ J mol}^{-1} \text{ K}^{-1}$ ($\text{PC}_{\text{ortho}}\text{-CH}_3$) listed in Tab. 5. For all fit parameters in Figs. 2-6 a qualitative agreement is obtained but differences are clearly outside experimental uncertainties. Because the accuracies of the experimental and the theoretical approach are hard to quantify we conclude that the experimental results are not inconsistent with the theoretical prediction that the two experimentally distinguished adducts are $\text{PC}_{\text{ortho}}\text{-C}_3\text{H}_7$ (adduct 1) and $\text{PC}_{\text{ortho}}\text{-CH}_3$ (adduct 2).

7. Conclusions

The reaction p-cymene + OH was reinvestigated using a reaction model assuming formation of two adduct species. This model results in triexponential OH decay curves in the presence of p-cymene that can be evaluated to extract the rate constants of the underlying reaction model. Despite the fact that the reaction between p-cymene and OH radicals can form four different adducts (two ipso-type and two ortho-type adducts) observed OH decays fit to that model within experimental error. Good agreement with literature data was found for the rate constant of OH reaction at room temperature. In a temperature range between 299 and 349 K Arrhenius expressions for rate constants of the reaction model were obtained, as well as the yields of the supposed two adducts. Thermodynamic data were derived from temperature dependent equilibrium constants. For one adduct reasonable results were obtained but for the second adduct the reaction enthalpy and reaction entropy are not within expectations and probably influenced by the presence of further adduct species. DFT calculations were made that indeed predict the formation of all four possible adducts with different yields. A full set of thermodynamic data for all relevant reactions was obtained. The formation of the two ortho-adducts was found to be predominant while the ipso-adducts are either almost negligible (ipso-CH_3) or react mostly by dealkylation rather than back-dissociation to OH and p-cymene ($\text{ipso-C}_3\text{H}_7$). This led to the conclusion that mainly the two ortho adducts were in equilibrium with OH and therefore detected in the experiments, resulting in triexponential OH decays. Finally, numerical simulations of OH decay curves were made using a combination of the theoretical results and measured OH rate constants. These decay curves were evaluated to quantify any departure from triexponential behavior and to reproduce the consequences of using the simplified reaction model. Results from these simulations show a qualitative agreement with experiments but differences are outside experimental uncertainties. The results from these simulations

show a reasonable agreement with experimental results confirming the theoretical prediction that two distinguished adducts are $\text{PC}_{\text{ortho}}\text{-C}_3\text{H}_7$ (adduct 1) and $\text{PC}_{\text{ortho}}\text{-CH}_3$ (adduct 2).

Acknowledgments

This work was supported by the Deutsche Forschungsgemeinschaft under grant ZE 792/6-1 and BO 1580/3-1, and by CNRS/INSU within the French-German CNRS-INSU/DFG bilateral program ATMOCHEM. We thank the research group of Roger Atkinson for the determination of the abstraction and dealkylation channels.

References

- S. D. Piccot, J. J. Watson and J. W. Jones, *Journal of Geophysical Research: Atmospheres*, 1992, **97**, 9897-9912.
- A. Guenther, C. N. Hewitt, D. Erickson, R. Fall, C. Geron, T. Graedel, P. Harley, L. Klinger, M. Lerdau, W. A. McKay, T. Pierce, B. Scholes, R. Steinbrecher, R. Tallamraju, J. Taylor and P. Zimmerman, *J. Geophys. Res.*, 1995, **100**, 8873-8892.
- R. Atkinson and J. Arey, *Atmos. Environ.*, 2003, **37**, 197-219.
- J. G. Calvert, *The Mechanisms of Atmospheric Oxidation of Aromatic Hydrocarbons*, Oxford University Press 2002.
- B. Bohn and C. Zetzsch, *Phys. Chem. Chem. Phys.*, 2012, **14**, 13933-13948.
- T. Berndt and O. Böge, *Int. J. Chem. Kinet.*, 2001, **33**, 124-129.
- J. von Buttlar, R. Koch, M. Siese and C. Zetzsch, *Geophysical Research Abstracts*, 2008, **10**.
- J.-C. Loison, M.-T. Rayez, J.-C. Rayez, A. Gratien, P. Morajkar, C. Fittschen and E. Villenave, *J. Phys. Chem. A*, 2012, **116**, 12189-12197.
- J. Noda, R. Volkamer and M. J. Molina, *J. Phys. Chem. A*, 2009, **113**, 9658-9666.
- D. F. Smith, C. D. McIver and T. E. Kleindienst, *J. Atmos. Chem.*, 1998, **30**, 209-228.
- S. M. Aschmann, J. Arey and R. Atkinson, *Atmos. Environ.*, 2010, **44**, 3970-3975.
- S. B. Corchnoy and R. Atkinson, *Environ. Sci. Technol.*, 1990, **24**, 1497-1502.
- P. Alarcon, R. Strekowski and C. Zetzsch, *Phys. Chem. Chem. Phys.*, 2013, **15**, 20105-20114.
- A. Wahner and C. Zetzsch, *J. Phys. Chem.*, 1983, **87**, 4945-4951.
- R. Koch, R. Knispel, M. Elend, M. Siese and C. Zetzsch, *Atmos. Chem. Phys.*, 2007, **7**, 2057-2071.
- S. Zhang, R. Strekowski, L. Bosland, A. Monod and C. Zetzsch, *Phys. Chem. Chem. Phys.*, 2011, **13**, 11671 - 11677.
- S. Zhang, R. S. Strekowski, L. Bosland, A. Monod and C. Zetzsch, *Int. J. Chem. Kinet.*, 2011, **43**, 547-556.
- Gaussian 09, Revision A.1*, M. J. Frisch, G. W. Trucks, H. B. Schlegel, G. E. Scuseria, M. A. Robb, J. R. Cheeseman, G. Scalmani, V. Barone, B. Mennucci, G. A. Petersson, H. Nakatsuji, M. Caricato, X. Li, H. P. Hratchian, A. F. Izmaylov, J. Bloino, G. Zheng, J. L. Sonnenberg, M. Hada, M. Ehara, K. Toyota, R. Fukuda, J. Hasegawa, M. Ishida, T. Nakajima, Y. Honda, O. Kitao, H. Nakai, T. Vreven, J. A. Montgomery, J. E. Peralta, F. Ogliaro, M. Bearpark, J. J. Heyd, E. Brothers, K. N. Kudin, V. N. Staroverov, R. Kobayashi, J. Normand, K. Raghavachari, A. Rendell, J. C. Burant, S. S. Iyengar, J. Tomasi, M. Cossi, N. Rega, J. M. Millam, M. Klene, J. E. Knox, J. B. Cross, V. Bakken, C. Adamo, J. Jaramillo, R. Gomperts, R. E. Stratmann, O. Yazyev, A. J. Austin, R. Cammi, C. Pomelli, J. W. Ochterski, R. L. Martin, K. Morokuma, V. G. Zakrzewski, G. A. Voth, P. Salvador, J. J. Dannenberg, S. Dapprich, A. D. Daniels, Farkas, J. B.

- Foresman, J. V. Ortiz, J. Cioslowski and D. J. Fox, eds., Wallingford CT 2009.
19. Y. Zhao and D. Truhlar, *Theor. Chem. Account*, 2008, **120**, 215-241.
- 5 20. R. Knispel, R. Koch, M. Siese and C. Zetzsch, *Ber. Bunsenges. Physikal. Chem*, 1990, **94**, 1375-1379.
21. R. Koch, PhD Dissertation, *Kinetische Untersuchung der Folgereaktionen der OH-Addukte von aromaten mit NO, NO₂ und O₂ mit simultaner Auswertung von Kurvenscharen*, University of Hannover, 1992.
- 10 22. R. Knispel, PhD Dissertation, *Reaktionen von OH-Radikalen mit Aromaten und Folgereaktionen entstandener OH-Addukte von Aromaten*, University of Hannover, 1993.
23. R. A. Perry, R. Atkinson and J. N. Pitts, *J. Phys. Chem.*, 1977, **81**, 296-304.
- 15 24. V. H. Uc, I. García-Cruz, A. Hernández-Laguna and A. Vivier-Bunge, *J. Phys. Chem. A*, 2000, **104**, 7847-7855.
25. I. Suh, D. Zhang, R. Zhang, L. T. Molina and M. J. Molina, *Chem. Phys. Lett*, 2002, **364**, 454-462.
- 20 26. D. Johnson, S. Raoult, R. Lesclaux and L. N. Krasnoperov, *J. Photoch. Photobio. A*, 2005, **176**, 98-106.
27. J. Fan and R. Zhang, *J. Phys. Chem. A*, 2006, **110**, 7728-7737.
28. J. M. Andino and A. Vivier-Bunge, in *Adv. Quantum. Chem.*, eds. E. G. Michael and S. J. Matthew, Academic Press 2008, vol. 55, pp. 297-310.
- 25 29. I. V. Tokmakov and M. C. Lin, *J. Phys. Chem. A*, 2002, **106**, 11309-11326.
30. M. R. Berman and M. C. Lin, *J. Phys. Chem.*, 1983, **87**, 3933-3942.
- 30

Cite this: DOI: 10.1039/c0xx00000x

www.rsc.org/pccp

PAPER